

Approximating Power Flow and Transmission Losses in Coordinated Capacity Expansion Problems

Fabian Neumann^{a,*}, Veit Hagenmeyer^a, Tom Brown^a

^a*Institute for Automation and Applied Informatics (IAI), Karlsruhe Institute of Technology (KIT),
Hermann-von-Helmholtz-Platz 1, 76344, Eggenstein-Leopoldshafen, Germany*

Abstract

With rising shares of renewables and the need to properly assess trade-offs between transmission, storage and sectoral integration as balancing options, building a bridge between energy system models and detailed power flow studies becomes increasingly important, but is computationally challenging.

In this paper, we compare both common and improved approximations for two nonlinear phenomena, power flow and transmission losses, in linear capacity expansion problems that co-optimize investments in generation, storage and transmission infrastructure. We evaluate different flow representations discussing differences in investment decisions, nodal prices, the deviation of optimised flows and losses from simulated AC power flows, and the computational performance. By using the open European power system model PyPSA-Eur, that combines high spatial and temporal resolution, we obtain detailed and reproducible results aiming at facilitating the selection of a suitable power flow model.

Given the differences in complexity, the optimal choice depends on the application, the user's available computational resources, and the level of spatial detail considered. Although the commonly used transport model can already identify key features of a cost-efficient system while being computationally performant, deficiencies under high loading conditions arise due to the lack of a physical grid representation. Moreover, disregarding transmission losses overestimates optimal grid expansion by 20%. Adding a convex relaxation of quadratic losses with two or three tangents to the linearised power flow equations and accounting for changing line impedances as the network is reinforced suffices to represent power flows and losses adequately in design studies. We show that the obtained investment and dispatch decisions are then sufficiently physical to be used in more detailed nonlinear simulations of AC power flow in order to better assess their technical feasibility. This includes determining reactive power flows and voltages, which the initial linear model neglects. Simpler approximations are less suitable for such ex-post analysis.

Keywords: energy system modelling, linear optimal power flow, transmission losses, capacity expansion planning, grid reinforcement

*Corresponding author

Email address: `fabian.neumann@kit.edu` (Fabian Neumann)

Preprint submitted to RSER

August 27, 2020

Contents

1	Introduction	3
2	Power System Planning Problem	4
3	Nonlinear Power Flow and Losses	6
3.1	Nonlinear AC Power Flow	6
3.2	Nonlinear Active Power Losses	6
3.3	Electrical Parameters of Transmission Lines	7
4	Linear Power Flow Models	7
4.1	Transport Model	9
4.2	Transport Model with Loss Approximation	9
4.3	Linearised Power Flow	10
4.4	Linearised Power Flow with Loss Approximation	11
4.5	Iterative Linearised Power Flow (with Loss Approximation)	14
5	Simulation Setup	14
5.1	Power System Model for Optimisation	14
5.2	Nonlinear AC Power Flow Simulation	15
6	Results and Discussion	16
6.1	Investments, Nodal Prices and Total System Costs	16
6.2	Validation of Loss Approximation	19
6.3	Validation of Optimised Line Flows	21
6.4	Computational Performance	24
6.5	Critical Appraisal	25
7	Conclusion	25
	References	26
Appendix A	AC Power Flow Problem Solved with Newton-Raphson	29
Appendix A.1	Without Distributed Slack	29
Appendix A.2	With Distributed Slack	29
Appendix B	Relations between Electrical Line Parameters	30
Appendix C	Additional Figures and Tables	30

1. Introduction

Energy system models seek to answer what infrastructure a future energy system requires for given policy goals, where and when it should be built, and how much it costs. For systems with high shares of renewable energy, the question to what extent the variability of weather-dependent wind and solar energy will be balanced in space with continent-spanning transmission networks and in time with storage and coupling to other energy sectors attracts much research. Because energy system models are frequently used in policy-making, it becomes crucial to understand their particular limitations.

To find credible answers for highly renewable systems, it has been demonstrated that models require coordinated expansion planning of generation, storage and transmission infrastructure because they strongly interact [1, 2]; high temporal resolution and scope to account for extreme weather events, storage operation, and investments shaped by the characteristic daily, synoptic and seasonal patterns of renewables and load [3, 4]; high spatial resolution and scope to also capture the spatio-temporal patterns, such as correlations of wind speeds across the continent, and to represent transmission constraints [5, 6]. As higher shares of renewables increase the frequency of transmission bottlenecks, more detailed grid modelling is needed that looks beyond import and export capacities but accounts for physical conditions such as loop flows, transmission losses, and curtailment due to otherwise overloaded lines [7, 8].

Especially for planning problems with both static investment and time-dependent dispatch variables spanning across thousands of operational conditions, a tractable yet sufficiently trustworthy representation of power flows is essential. Ideally, outputs are detailed enough to be used as inputs for more accurate analyses, bridging the granularity gap between coarsely-resolved planning models and more detailed engineering models. Yet, even in strategic problems speed matters for performing pivotal sensitivity analyses; e.g. regarding uncertain cost parameters, reference weather years, technology choices, and resource boundaries. Unfortunately, the first-choice AC power flow equations are nonlinear and nonconvex, which makes the embedded AC optimal power flow problem NP-hard [9–11].

Even for a linear representation of power flows, considerations of transmission expansion planning result in a bilinear problem because line impedances change as line capacities are increased. While we can deal with this challenge through iterative impedance updates in sequential linear programming [12], the problem would become even more complex if a discrete set of transmission expansion plans were considered, rather than continuous line expansion. More generally, we can approach computational challenges from multiple angles: by improving solving algorithms or by figuring out what model details can be simplified while retaining accuracy [13]. Examples include the level of spatial aggregation, temporal aggregation, technology detail and diversity, or finally the approximation of power flow.

The transport model, that takes account only of power transfer capacities while ignoring impedances, and the linearised power flow model, which includes impedances to consider both Kirchhoff laws but no losses, are commonly used in energy system models. Among the models reviewed by Ringkjøb et al. [14] around four in five models use a transport model if flows are represented, whereas only one in five uses a linearised power flow model. Previous work has compared these two major variants [15–18], and some performed simulations of AC power flow after optimisation [18, 19]. The comparisons indicate little discrepancy regarding total system cost and cross-border transmission, but also differences in nodal prices and overlooked line overloadings when checked against AC power flow calculations. However, the cogency of existing comparisons is limited by the use of low spatial resolution models with fewer than

25 nodes. Furthermore, the consideration of losses is underrepresented in design studies, but alongside characteristic weather patterns shapes the tradeoffs regarding the volume of transmitted energy because losses increase as more power is transported [20, 21].

In the present contribution, we offer a comprehensive comparison of linear representations of power flow and losses in theory and practice. We outline their characteristic benefits and shortcomings in the context of coordinated capacity expansion problems, where generation, transmission and storage infrastructure is jointly planned. Given the multitude of modelling uncertainties, we assess under which circumstances it is worth embedding more elaborate flow models than a simple transport model. We further extend beyond previous research by introducing a computationally inexpensive loss approximation that incorporates an efficient reformulation of the linearised power flow equations based on a cycle decomposition of the network graph. By using an open model of the European power system, PyPSA-Eur [22], spanning the whole continent with hundreds of nodes and hourly temporal coupling due to the consideration of storage units, we achieve advanced and reproducible comparisons in systems with high shares of renewables.

The content complements the best practices of energy system modelling, characterised in Pfenniger et al. [23] and DeCarolis et al. [24], regarding the choice of suitable power flow models. While we take an investment planning perspective in this paper, we underline that the way that the transmission of power is represented is relevant beyond system planning. For instance, it plays a role in the design of future electricity markets with multiple bidding zones and flow-based market coupling [17, 25, 26].

We structured this contribution as follows. We begin with an introduction to the basic long-term power system planning problem in Section 2 and briefly review the physics of power flow in Section 3. We continue with the different linear power flow representations in Section 4. Section 5 presents the experimental setup, the results of which are discussed and critically appraised in Section 6. Section 7 concludes this paper with a summary and recommendations.

2. Power System Planning Problem

This section presents the full long-term power system planning problem. We confine the formulation to the power system, but it can also serve to represent the power system embedded within the full energy system. The representation of power flows is one decisive constituent component and its variants are later introduced in the context of this problem in Section 4.

The objective is to minimize the total annual system costs, comprising annualised¹ capital costs c_* for investments at locations i in generator capacity $G_{i,r}$ of technology r , storage power capacity $H_{i,s}$ of technology s , and transmission line capacities P_ℓ , as well as the variable operating costs o_* for generator dispatch $g_{i,r,t}$:

$$\min_{G,H,F,g} \left[\sum_{i,r} c_{i,r} \cdot G_{i,r} + \sum_{i,s} c_{i,s} \cdot H_{i,s} + \sum_{\ell} c_{\ell} \cdot P_{\ell} + \sum_{i,r,t} w_t \cdot o_{i,r} \cdot g_{i,r,t} \right] \quad (1)$$

where representative time snapshots t are weighted by the time span w_t such that their total duration adds up to one year; $\sum_{t \in \mathcal{T}} w_t = 365 \cdot 24\text{h} = 8760\text{h}$. The objective function is subject to

¹The annuity factor $\frac{1-(1+\tau)^{-n}}{\tau}$ converts the overnight investment of an asset to annual payments considering its lifetime n and cost of capital τ .

a set of linear constraints, including multi-period linear optimal power flow (LOPF) equations, resulting in a linear programme (LP).

The capacities of generation, storage and transmission infrastructure are constrained above by their installable potentials and below by any existing components:

$$\underline{G}_{i,r} \leq G_{i,r} \leq \overline{G}_{i,r} \quad \forall i, r \quad (2)$$

$$\underline{H}_{i,s} \leq H_{i,s} \leq \overline{H}_{i,s} \quad \forall i, s \quad (3)$$

$$\underline{P}_\ell \leq P_\ell \leq \overline{P}_\ell \quad \forall \ell \quad (4)$$

The dispatch of a generator may not only be constrained by its rated capacity but also by the availability of variable renewable energy, which may be derived from reanalysis weather data. This can be expressed as a time- and location-dependent availability factor $\overline{g}_{i,r,t}$, given per unit of the generator's capacity:

$$0 \leq g_{i,r,t} \leq \overline{g}_{i,r,t} G_{i,r} \quad \forall i, r, t \quad (5)$$

The dispatch of storage units is split into two positive variables; one each for charging $h_{i,s,t}^+$ and discharging $h_{i,s,t}^-$. Both are limited by the power rating $H_{i,s}$ of the storage units.

$$0 \leq h_{i,s,t}^+ \leq H_{i,s} \quad \forall i, s, t \quad (6)$$

$$0 \leq h_{i,s,t}^- \leq H_{i,s} \quad \forall i, s, t \quad (7)$$

The energy levels $e_{i,s,t}$ of all storage units have to be consistent with the dispatch in all hours.

$$e_{i,s,t} = \eta_{i,s,0}^{w_t} \cdot e_{i,s,t-1} + w_t \cdot h_{i,s,t}^{\text{inflow}} - w_t \cdot h_{i,s,t}^{\text{spillage}} + \eta_{i,s,+} \cdot w_t \cdot h_{i,s,t}^+ - \eta_{i,s,-}^{-1} \cdot w_t \cdot h_{i,s,t}^- \quad \forall i, s, t \quad (8)$$

Storage units can have a standing loss $\eta_{i,s,0}$, a charging efficiency $\eta_{i,s,+}$, a discharging efficiency $\eta_{i,s,-}$, natural inflow $h_{i,s,t}^{\text{inflow}}$ and spillage $h_{i,s,t}^{\text{spillage}}$. The storage energy levels are assumed to be cyclic

$$e_{i,s,0} = e_{i,s,|T|} \quad \forall i, s \quad (9)$$

and are constrained by their energy capacity

$$0 \leq e_{i,s,t} \leq \overline{T}_s \cdot H_{i,s} \quad \forall i, s, t. \quad (10)$$

To reduce the number of decision variables, we link the energy storage volume to power ratings using a technology-specific parameter \overline{T}_s that describes the maximum duration a storage unit can discharge at full power rating.

Total CO₂ emissions may not exceed a target level Γ_{CO_2} . The emissions are determined from the time-weighted generator dispatch $w_t \cdot g_{i,r,t}$ using the specific emissions ρ_r of fuel r and the generator efficiencies $\eta_{i,r}$

$$\sum_{i,r,t} \rho_r \cdot \eta_{i,r}^{-1} \cdot w_t \cdot g_{i,r,t} \leq \Gamma_{\text{CO}_2}. \quad (11)$$

All power flows $p_{\ell,t}$ are also limited by their capacities P_ℓ

$$|p_{\ell,t}| \leq \overline{P}_\ell P_\ell \quad \forall \ell, t, \quad (12)$$

where \bar{p}_ℓ acts as a per-unit security margin on the line capacity to allow a buffer for the failure of single circuits ($N - 1$ condition) and reactive power flows.

Ultimately, we need constraints that define the power flows $p_{\ell,t}$ in the network. In the next Section 3, we briefly set foundations for nonlinear power flow and losses. The various alternative flow models are then presented in Section 4. The subsequent descriptions will omit the time index t for notational simplicity.

3. Nonlinear Power Flow and Losses

This section briefly revises the nonlinear AC power flow equations, important electrical parameters of transmission lines, and how to calculate active power losses on a line. We do this to set the foundations for derivations of the covered flow models.

3.1. Nonlinear AC Power Flow

The active power flow $p_{\ell(i,j)}$ of a line $\ell \equiv \ell(i,j)$ from bus i to bus j can be described in voltage-polar coordinates by

$$p_{\ell(i,j)} = g_\ell |V_i|^2 + |V_i| |V_j| [g_\ell \cos(\theta_i - \theta_j) - b_\ell \sin(\theta_i - \theta_j)] \quad (13)$$

and, analogously, the reactive power flow $q_{\ell(i,j)}$ is given by

$$q_{\ell(i,j)} = b_\ell |V_i|^2 + |V_i| |V_j| [g_\ell \sin(\theta_i - \theta_j) - b_\ell \cos(\theta_i - \theta_j)], \quad (14)$$

where $|V_i|$ is the per-unit bus voltage magnitude, θ_i is the bus voltage angle, g_ℓ is the line conductance, and b_ℓ is the line susceptance [27].

3.2. Nonlinear Active Power Losses

To derive an expression for the active power losses in a transmission line, we apply the convention that departing power flows are positive and arriving power flows are negative. Consequently, if power flows from bus i to j , $p_{\ell(i,j)} > 0$ and $p_{\ell(j,i)} < 0$. The losses ψ_ℓ are the difference between power sent and power received [27], therefore

$$\psi_\ell = p_{\ell(i,j)} + p_{\ell(j,i)}. \quad (15)$$

Substituting equation (13) into equation (15) yields

$$\psi_\ell = g_\ell |V_i|^2 + |V_i| |V_j| [g_\ell \cos(\theta_i - \theta_j) - b_\ell \sin(\theta_i - \theta_j)] \quad (16)$$

$$+ g_\ell |V_j|^2 + |V_j| |V_i| [g_\ell \cos(\theta_j - \theta_i) - b_\ell \sin(\theta_j - \theta_i)] \quad (17)$$

and using the trigonometric identities $\cos(-\alpha) = \cos(\alpha)$ and $\sin(-\alpha) = -\sin(\alpha)$ translates to

$$\psi_\ell = g_\ell |V_i|^2 + |V_i| |V_j| [g_\ell \cos(\theta_i - \theta_j) - b_\ell \sin(\theta_i - \theta_j)] \quad (18)$$

$$+ g_\ell |V_j|^2 + |V_j| |V_i| [g_\ell \cos(\theta_i - \theta_j) + b_\ell \sin(\theta_i - \theta_j)]. \quad (19)$$

We can further simplify this expression to the loss formula

$$\psi_\ell = g_\ell (|V_i|^2 + |V_j|^2) - 2 |V_i| |V_j| g_\ell \cos(\theta_i - \theta_j). \quad (20)$$

We will use this formula in Section 4.4 to derive a linear approximation for losses.

Model	Section	Variables	Eq. Constraints	Ineq. Constraints
Transport	4.1	$ \mathcal{L} $	$ \mathcal{N} - 1$	0
Lossy Transport	4.2	$2 \mathcal{L} $	$ \mathcal{N} - 1$	0
Linearised Power Flow	4.3	$ \mathcal{L} $	$ \mathcal{L} $	0
Linearised Power Flow with Loss Approximation	4.4	$2 \mathcal{L} $	$ \mathcal{L} $	$2n \mathcal{L} $

Table 1: Comparison of the number of variables and equality/inequality constraints related to flow models per snapshot $t \in \mathcal{T}$. The constraint count excludes variable bounds. $|\mathcal{L}|$ is the number of lines, $|\mathcal{N}|$ is the number of nodes, and $2n$ represents the number of tangents used for the loss approximation.

3.3. Electrical Parameters of Transmission Lines

The complex per-unit impedance $z_\ell = r_\ell + ix_\ell$ is composed of resistance r_ℓ and reactance x_ℓ . Likewise, the admittance $y_\ell = g_\ell + ib_\ell$ is composed of conductance g_ℓ and susceptance b_ℓ . Impedance and admittance are reciprocals ($y_\ell = z_\ell^{-1}$). Hence, if we assume a dominance of reactance over ohmic resistance ($r_\ell \ll x_\ell$), as applies for high voltage overhead transmission lines, we obtain the approximations

$$g_\ell \approx \frac{r_\ell}{x_\ell^2}, \quad (21)$$

$$b_\ell \approx \frac{1}{x_\ell}. \quad (22)$$

For a derivation, see [Appendix B](#). We will use these relations in [Section 4.3](#) and [Section 4.4](#). In view of the approximation of line losses in later sections, note that although we assume that resistance is dominated by reactance, we do not assume resistance to be zero (cf. [\[28, 29\]](#)).

4. Linear Power Flow Models

The AC power flow equations [\(13\)](#) are nonlinear and nonconvex. This is challenging because multiple local minima exist due to the trigonometric expressions and when directly incorporated in the optimisation problem they would make the problem NP-hard [\[9–11\]](#). To be able to run large optimisation problems of the continental power system at sufficient spatial and temporal resolution it is hence inevitable to retain a convex problem that can be solved in polynomial time and does not possess local minima.

In this section we describe and develop various linear representations of power flow. These are introduced in the order from least to most accurate, progressively increasing the complexity; namely (i) the common transport model, (ii) a lossy transport model, (iii) the lossless linearised power flow, and (iv) a lossy linearised power flow model. [Figure 4](#) shows the relations between the formulations and [Table 4](#) documents differences in the number of variables and constraints. The scope of this work is deliberately constrained to:

- *only linear problems*: To avail of powerful, scalable and fast interior-point solvers, and to guarantee an optimal solution, we only include formulations that entail linear problems. However, there exist promising second-order cone or semidefinite convex relaxations of the power flow equations. For excellent theoretical reviews of convex relaxations and approximations of power flow see [Molzahn et al. \[30\]](#), [Taylor \[27\]](#), and [Coffrin et al. \[31\]](#).

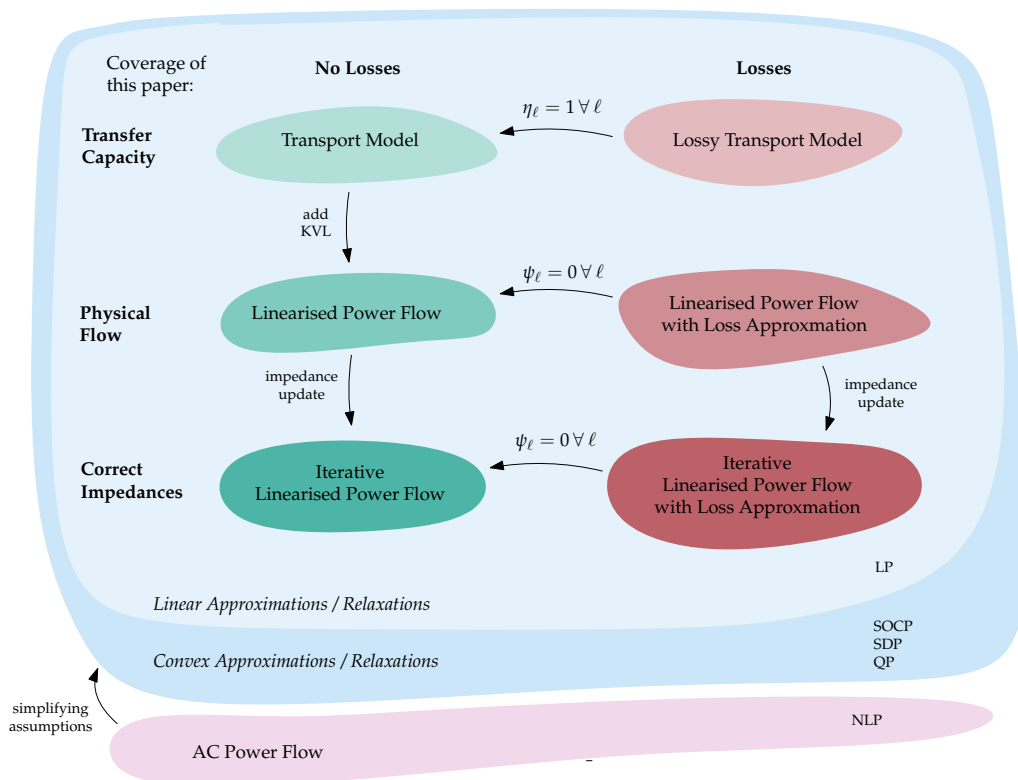


Figure 1: Illustration of the scope of the present paper and its context. It shows the connections between the covered linear power flow models, their main features, and how they are related to other (convexified) nonlinear formulations.

- *only active power*: We furthermore confine our analysis to formulations that do not capture reactive power flows or information on bus voltages. Nonetheless, linear problems that capture selected aspects of this are under active research; see e.g. Coffrin et al. [32].
- *only comparison of different feasible spaces*: We compare different linear flow models that define different feasible spaces. We do not compare equivalent reformulations of identical models, since this has been analysed in Hrsch et al. [33].
- *no copper plate model*: Although occasionally encountered in generation and storage capacity expansion models, we do not include the copper plate relaxation in our comparisons because it does not capture information on power flows in transmission networks. The copper plate model removes all lines and aggregates all components to a single node. It is a relaxation because any transmission of power becomes unconstrained and incurs no cost. For the impact of spatial clustering – of which the copper plate model is the extreme – on optimal investments we refer to Hrsch et al. [5].

4.1. Transport Model

The transport model is also known as a network flow model, trade model, transshipment model or net transfer capacity (NTC) model [27]. It ignores the effect of impedances on flows (including losses) and, besides the capacity constraints of lines, only requires nodal power balance according to Kirchhoff’s Current Law (KCL); i.e. the power injected at each bus must equal the power withdrawn by attached lines

$$p_i = \sum_{\ell} K_{i\ell} p_{\ell} \quad \forall i \in \mathcal{N}, \quad (23)$$

where p_i is the active power injected or consumed at node i and K is the incidence matrix of the network graph which has non-zero values +1 if line ℓ starts at bus i and -1 if line ℓ ends at bus i .

Because the columns of the incidence matrix each sum up to zero, KCL yields $|\mathcal{N}|-1$ linearly independent constraints. These are not sufficient to uniquely determine the $|\mathcal{L}|$ unknown flows. The transport model allows arbitrary flows as long as flow conservation is fulfilled, also because it is free and lossless to transmit power. This makes the transport model degenerate, which can be detrimental to the solving speed. Also, of course, this does not adequately reflect the physical behaviour of power flows in the transmission network.

Despite its drawbacks, the transport model is very popular. In the comprehensive review by Ringkjøb et al. [14], it is applied in a majority of models. This minimalistic representation of flows is useful to develop an understanding for the potential of increased transfer capacity between regions, rather than assessing specific transmission bottlenecks and reinforcement needs. It is often applied in investment models where the grid is highly aggregated to a few nodes (e.g. one node per country in Europe or federal state in the United States) or analyses of energy markets across multiple bidding zones. Its main advantages are ease of implementation and fast solving speed. For pure dispatch problems without investment decisions one can even utilise specialised network flow algorithms; for instance the minimum cost flow algorithm [34].

4.2. Transport Model with Loss Approximation

Part of the drawbacks and degeneracy of the transport model stems from the disregard of transmission losses. As partial remedy, we can amend the transport model with a simple loss

approximation which assumes lines to have a constant transmission efficiency η_ℓ depending on their length. In this case, the power arriving at the receiving bus is lower than the power injected at the sending bus. To differentiate between sending bus and receiving bus, we need to split the bidirectional power flow variable p_ℓ into forward flows p_ℓ^+ and backward flows p_ℓ^- with capacity limits

$$0 \leq p_\ell^+ \leq \bar{p}_\ell P_\ell \quad \forall \ell \in \mathcal{L} \quad (24)$$

$$0 \leq p_\ell^- \leq \bar{p}_\ell P_\ell \quad \forall \ell \in \mathcal{L} \quad (25)$$

which substitute the variables p_ℓ and their bounds given in equation (12). Furthermore, we need to adjust the nodal balance constraints (23) to reflect the transmission losses and separated power flow variables to

$$p_i = \sum_\ell K_{i\ell}^+ p_\ell^+ - \sum_\ell K_{i\ell}^- p_\ell^- \quad \forall i \in \mathcal{N}, \quad (26)$$

where K^+ is the lossy incidence matrix of the network graph regarding forward flows p_ℓ^+ which has non-zero values +1 if line ℓ starts at bus i and $-\eta_\ell$ if line ℓ ends at bus i . Analogously, K^- regards backward flows p_ℓ^- with non-zero values η_ℓ if line ℓ starts at bus i and -1 if line ℓ ends at bus i .

The transmission losses alleviate some degeneracy of the transport model since considering losses yields an incentive to minimise power flows rather than to distribute them arbitrarily. However, this is paid for with a doubling in the number of flow variables. Additionally, while the use of a constant transmission efficiency is an improvement from the plain transport model, it still ignores the quadratic relationship between power flow and losses [20]. Note, that if all lines have no losses ($\eta_\ell = 1$), the lossy transport model is equivalent to the regular transport model.

4.3. Linearised Power Flow

The linearised power flow model, which is also known as linearised load flow, DC power flow or B Θ model, extends the lossless transport model. In addition to the nodal power balance constraints (23) from KCL and capacity limits (12), linear constraints for Kirchhoff's Voltage Law (KVL) are included, which define how power flows split in parallel paths. We derive these by simplifying the nonlinear power flow equations (13) and (14). Assuming

- all per-unit voltage magnitudes are close to one ($|V_i| \approx 1$),
- conductances g_ℓ are negligible relative to susceptances b_ℓ ($b_\ell \gg g_\ell$),
- voltage angle differences are small enough ($\sin(\theta_i - \theta_j) \approx \theta_i - \theta_j$ and $\cos(\theta_i - \theta_j) \approx 0$),
- reactive power flows q_ℓ are negligible compared to real power flows p_ℓ ($q_\ell \approx 0$),

leads to

$$p_\ell = b_\ell(\theta_i - \theta_j), \quad (27)$$

and when we further assume $r_\ell \ll x_\ell$, by substituting (22) we obtain

$$p_\ell = \frac{\theta_i - \theta_j}{x_\ell}. \quad (28)$$

This angle-based formulation is the most common linear formulation of KVL [27]. But it is possible to avoid the auxiliary voltage angle variables and reduce the required number of constraints by using a cycle basis of the network graph [33]. Namely, KVL states that the sum of voltage angle differences across lines around all cycles in the network must sum up to zero. Considering a set of independent cycles c of the network forming a cycle basis, which are expressed as a directed linear combination of the lines ℓ in a cycle incidence matrix

$$C_{\ell c} = \begin{cases} 1 & \text{if edge } \ell \text{ is element of cycle } c, \\ -1 & \text{if reversed edge } \ell \text{ is element of cycle } c, \\ 0 & \text{otherwise,} \end{cases} \quad (29)$$

KVL is formulated by

$$\sum_{\ell} C_{\ell c}(\theta_i - \theta_j) = 0 \quad \forall c \in C. \quad (30)$$

Using equation (28), we can express KVL directly in terms of the power flows and circumvent the auxiliary voltage angle variables

$$\sum_{\ell} C_{\ell c} p_{\ell} x_{\ell} = 0 \quad \forall c \in C. \quad (31)$$

Although less common, this cycle-based formulation (31) has been shown to significantly outperform the angle-based formulation (28) [33, 35]. There are even further equivalent reformulations of the linearised power flow [33]; for example the Power Transfer Distribution Factor (PTDF) formulation, which directly relates nodal power injections to line flows. Because our focus lies on the comparison of different flow models, not their diverse reformulations, we only evaluate the computationally performant cycle-based formulation in the present contribution.

With the cycle-based formulation one can clearly see that the transport model is equivalent to the linearised power flow in radial networks; i.e. when the network has no cycles. Also, the absence of auxiliary voltage angle variables facilitates the insight that the transport model is a relaxation of the linearised power flow because the latter only adds constraints in the same variable space.

The linearised power flow model is claimed to be accurate when reactance dominates ($x_{\ell} \gg r_{\ell}$) and when parallel lines have similar ratios [36], but very long lines in highly aggregated networks can deteriorate the quality of the approximation (see Section 6.3). An advantage of this model over the transport model is that it captures some meaningful physical characteristics observed in the operation of electrical grids. Namely, it is capable of revealing loop flows in meshed networks; for instance recurring spillover effects between Germany and the Czech Republic. Nevertheless, it still disregards losses.

If we would consider that lines can be built between buses where there are currently none, another variant is the so-called hybrid model. This version formulates linearised power flow constraints for existing lines and employs a transport model for candidate lines.

4.4. Linearised Power Flow with Loss Approximation

Neglecting resistive losses is considered to be among the largest sources of error in the linearised power flow formulation, particularly in large networks [36]. The following extension of the lossless linearised power flow (Section 4.3) is a mixture of similar variants encountered in the literature with a focus on computational efficiency. We reference where we follow or

deviate from previous work below. This or similar formulations have rarely been applied in the co-optimisation of transmission, storage and generation capacities, but rather in detailed operational optimal power flow (OPF) or transmission expansion planning (TEP) problems; see overview in [7].

We start by adding a loss variable ψ_ℓ for each line. Losses reduce the effective transmission capacity of a line

$$|p_\ell| \leq \bar{p}_\ell P_\ell - \psi_\ell \quad (32)$$

and must be accounted for in the nodal balance equation (23)

$$p_i = \sum_\ell K_{i\ell} p_\ell + \frac{|K_{i\ell}|}{2} \psi_\ell \quad \forall i \in \mathcal{N}. \quad (33)$$

We split the losses ψ_ℓ equally between both buses (like in [37–39]) and do not allocate them at the sending bus exclusively (like in [29, 40]). The latter could be modelled with an absolute value function in the linear problem. However, this would involve splitting flow and loss variables each into positive and negative segments. Because this adds many auxiliary decision variables, we decided in favor of distributing the losses evenly. This choice is paid for with the possibility of overestimating losses due to an extensive convex relaxation.

Assuming close to nominal per-unit voltage magnitudes $|V_i| \approx 1$ the loss formula given in equation (20) becomes

$$\psi_\ell = 2g_\ell [1 - \cos(\theta_i - \theta_j)]. \quad (34)$$

This is the basis for the linearised loss formulation in [39]. We can also express this in terms of active power flows p_ℓ by substituting equation (28) into equation (34)

$$\psi_\ell = 2g_\ell [1 - \cos(p_\ell x_\ell)]. \quad (35)$$

This makes the loss formulation independent from the voltage angle variables and we can therefore avail of the speed-up obtained by using the cycle-based formulation (31).

Using the small-angle approximation $\cos(\alpha) \approx 1 - \alpha^2/2$, equation (35) becomes quadratic

$$\psi_\ell = 2g_\ell \left[1 - \left(1 - \frac{(p_\ell x_\ell)^2}{2} \right) \right] = g_\ell (p_\ell x_\ell)^2. \quad (36)$$

By inserting equation (21) we get

$$\psi_\ell = \frac{r_\ell}{x_\ell^2} (p_\ell x_\ell)^2 \quad (37)$$

or simply

$$\psi_\ell = r_\ell p_\ell^2. \quad (38)$$

This is the basis for the linearised loss formulation in [29]. Equation (38) is still a quadratic equality constraint, and therefore nonconvex. Other works have discussed or applied a piecewise linearisation of equation (38) [30, 38, 39, 41, 42]. But because the use of integer variables to define the segments would entail a nonconvex mixed-integer problem (MILP), we choose not to pursue this approach. Instead, by building a convex envelope around this constraint from the upper and lower bounds for ψ_ℓ as well as a number of tangents as inequality constraints, we can incorporate transmission losses while retaining a linear optimisation problem. This is illustrated in Figure 2. For setting the lower limit, by definition losses are positive

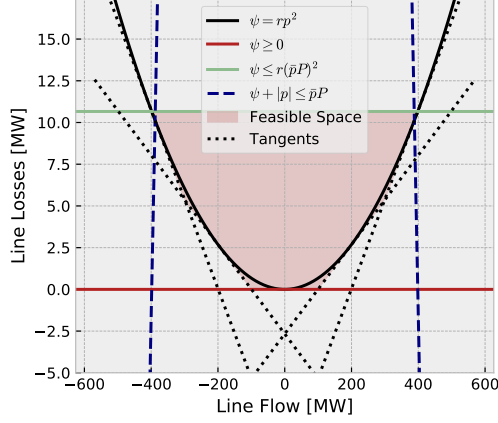


Figure 2: Illustration of the feasible space in the flow-loss ($p_\ell - \psi_\ell$) dimensions.

$$\psi_\ell \geq 0 \quad (39)$$

and by substituting maximal line flows

$$p_\ell \leq \bar{p}_\ell P_\ell \leq \bar{p}_\ell \bar{P}_\ell \quad (40)$$

into (38) we obtain the upper limit

$$\psi_\ell \leq r_\ell (\bar{p}_\ell \bar{P}_\ell)^2. \quad (41)$$

Next, we derive $2n$ evenly spaced (like in [30]) mirrored tangents which approximate equation (38) as inequalities from below. These have the form

$$\psi_\ell \geq m_k \cdot p_\ell + a_k \quad \forall k = 1, \dots, n \quad (42)$$

$$\psi_\ell \geq -m_k \cdot p_\ell + a_k \quad \forall k = 1, \dots, n \quad (43)$$

At segment k we calculate the losses

$$\psi_\ell(k) = r_\ell \left(\frac{k}{n} \cdot \bar{p}_\ell \bar{P}_\ell \right)^2 \quad (44)$$

and the corresponding slope

$$m_k = \frac{d\psi_\ell(k)}{dk} = 2r_\ell \left(\frac{k}{n} \cdot \bar{p}_\ell \bar{P}_\ell \right) \quad (45)$$

and the offset

$$a_k = \psi_\ell(k) - m_k \left(\frac{k}{n} \cdot \bar{p}_\ell \bar{P}_\ell \right). \quad (46)$$

Together, equations (39), (41), (42), and (43) form a convex envelope of equation (38).

A recurring criticism of this extensive convex relaxation is the possibility of so-called fictitious or artificial losses [30, 43–46]. As illustrated by Figure 2, the model does indeed allow

for overestimating losses. This can be economical if negative locational marginal prices occur. Overestimating losses is equivalent to dissipating power at a node. Another component in the problem formulation that already permits this behaviour are storage units (see equations (6)–(8)). To avoid binary variables, storage units may charge and discharge at the same time. Power is then lost by cycling through the conversion efficiencies. We argue that fictitious losses are not problematic because (i) negative nodal prices are rare, (ii) such behaviour could be realised in operation by low-cost resistors and demand response, and (iii) the loss overestimation is bounded. We will substantiate this argument with experimental results in Section 6.2.

4.5. Iterative Linearised Power Flow (with Loss Approximation)

When using the linearised power flow, with and without losses (Sections 4.3 and 4.4), the impedances of transmission lines affect the flows and losses. The relations of reactances x_ℓ determine the distribution of flows (cf. equation (31)). The resistances r_ℓ set the losses (cf. equation (38)). Thus, for reactances we are only interested in relative values, whereas for the resistances the absolute values are decisive.

Line impedances change as line capacities are increased ($x_\ell \propto 1/P_\ell$ and $r_\ell \propto 1/P_\ell$). Ignoring this dependency would result in distorted power flows. Expanded lines would experience less flow than they should. Losses may also be overestimated as the extension of parallel lines reduces the effective resistance.

Consequently, the representation of grid physics is improved by taking account of the relation between line capacities and impedances, yet also complicates the problem. If we considered discrete expansion options we would use a big- M disjunctive relaxation to resolve the nonlinearity [35]. But since we assume continuous line expansion in view of computational performance, we instead pursue an iterative heuristic approach. In previous works, we have shown that this is an acceptable approximation [12].

We sequentially solve the optimisation problem from Section 2 and in each iteration update the line impedances according to their optimised capacities. We repeat this process until (i) line expansion choices do not change in subsequent iterations and convergence is reached, or (ii) a predetermined number of iterations are performed. In the latter case, the final iteration should be run with fixed line capacities such that impedances do not change anymore.

5. Simulation Setup

Having developed the individual power flow models in theory, this section outlines the setup we use to test them. First, we introduce the power system model in Section 5.1 for which we optimise investments. Second, we outline the methodology we use to validate the resulting approximated line flows in Section 5.2.

5.1. Power System Model for Optimisation

We evaluate the different flow models on the open power system dataset PyPSA-Eur (v0.1.0), which covers the whole European transmission system [22]. We choose a spatial resolution of 250 nodes and a temporal resolution of 4380 snapshots, one for every two hours of a full year. This reflects the maximum for which all flow models presented in Section 4 could be solved.

Targeting an emission reduction of 100% in the power sector, we only consider renewable resources [47]. Following the problem formulation from Section 2, solar PV, onshore and offshore

wind capacities are co-optimised with battery storage, hydrogen storage, and transmission infrastructure in a greenfield planning approach, subject to spatio-temporal capacity factors and geographic potentials. Exceptions to greenfield planning are existing transmission infrastructure, which can only be reinforced but not removed, and today’s run-of-river and hydropower capacities including pumped hydroelectric energy storage, which are not extendable due to assumed geographical constraints. HVDC links are assumed to have losses of 3% per 1000 km [48] and can be expanded continuously up to 20 GW (each composed of several smaller parallel circuits). Planned projects from the 2018 Ten Year Network Development Plan (TYNDP) are included [49]. We only apply link losses to flow models which also account for losses in HVAC lines. HVAC line capacity can also be expanded continuously; by the maximum of doubled capacity or additional 5 GW. When using the lossy transport model, HVAC lines are assumed to have constant losses in the order of 5% per 1000 km [48]. To approximate $N - 1$ security, lines may only be used up to 70% of their nominal rating. More details are provided in Hirsch et al. [22].

Technically, the optimisation problem is implemented using the free Python modelling framework PyPSA (v0.17.0) working with the Pyomo interface [50]. Both optimality and feasibility tolerances are set to a value of 0.1%, which is sufficient given the mentioned approximations made in the model. We use the cycle-based formulation of Kirchhoff’s Voltage Law for any model that accounts for it. The code to reproduce the experiments is openly available at github.com/fneum/power-flow-models.

In accordance with descriptions in Section 4, the following flow models are evaluated:

- lossless transport model as TRANSPORT,
- lossy transport model as LOSSY TRANSPORT,
- lossless linearised power flow with no iterations as LOSSLESS,
- lossless linearised power flow with 3 iterations as ITERATIVE LOSSLESS,
- lossy linearised power flow with 6 tangents and no iterations as LOSSY, and
- lossy linearised power flow with 6 tangents and 3 iterations as ITERATIVE LOSSY.

5.2. Nonlinear AC Power Flow Simulation

All presented flow models approximate the AC power flow equations (Section 3). Thus, to identify possibly overlooked line overloading, and to demonstrate characteristic features of particular flow models, we use the AC power flow equations to assess the quality of the respective approximations.

We compare optimised flows to simulated flows which we obtain by solving the AC power flow equations ex-post based on the optimised dispatch of controllable system components. Specifically, we do not reoptimise dispatch decisions subject to the AC power flow model due to computational constraints given such large multi-period problems, but only check their feasibility. We use the Newton-Raphson method (see e.g. [51]) and distribute the total slack power across all buses in proportion to their total generation capacity [21, 52] (details are provided in Appendix A). Moreover, we consider PV buses² at each node since the reactive power set points

²For PV buses, the nodal active power injections p_i and voltage magnitudes $|V_i|$ are known (we assume nominal voltage magnitudes $|V_i| = 1$). Bus voltage angles θ_i and reactive power feedin q_i are to be found. Conversely, for PQ buses the nodal active power injections p_i and reactive power injections q_i are known. Bus voltage magnitudes $|V_i|$ and angles θ_i are to be found.

Indicator	Unit	Lossy			Iterative		Iterative
		Transport	Transport	Lossless	Lossless	Lossy	
System cost	bn€p.a.	220.2	226.2	224.9	225.7	243.8	238.5
	€/MWh	70.2	72.1	71.7	71.9	77.7	76.0
Energy transmitted	EWhkm	1.56	1.26	1.36	1.28	0.90	0.94
Network expansion	TWkm	216	214	206	206	160	170
Transmission losses	% of load	0	2.3	0	0	5.1	3.7
Curtailment	%	2.0	1.9	2.3	2.4	2.2	2.4
Share of $ \theta_i - \theta_j \geq 30^\circ$	%	5.1	3.7	4.6	3.9	1.4	1.5

Table 2: Various statistical indicators compared across covered flow models.

are unknown. Hence, we assume there to be sufficient reactive power control infrastructure to maintain nominal voltages. We argue that in systems with high shares of renewables the PV bus assumption is justified in view of a growing number of distributed power generation units, each capable of contributing to voltage control by reactive power injection or consumption, and power electronic devices such as Flexible Alternating Current Transmission Systems (FACTS). While the linearised power flow approximations neglect the shunt capacitance of lines, these are taken into account in the subsequent AC power flow simulation according to the standard equivalent Π model [53]. Suitable short- to medium-length lines between 25km and 250km make up about 85% of all lines in the model (Figure C.15). The remaining 15% of lines, which are longer than 250km, are modelled identically although more rigorous alternatives exist. These include partitioning long lines into multiple shorter sections to model series compensation [53], or using equations specifically for long lines that include fewer simplifying approximations of impedances than the Π model [54].

6. Results and Discussion

This section presents and discusses the results from the experiments as described in Section 5. As evaluation criteria we consider the total system costs and the optimal system composition (Section 6.1), the error of optimised losses (Section 6.2), the error of optimised flows compared to simulated flows (Section 6.3), as well as peak memory consumption and solving time (Section 6.4).

6.1. Investments, Nodal Prices and Total System Costs

Table 2 presents total transmission losses to sum up to around 4% of the total load when updated impedances according to line expansion are used. In comparison to the 1.2% transmission losses reported by the German Federal Network Agency for the year 2019 [55], this value is higher owing to the larger volume of power transmission across the whole continent in scenarios with high shares of renewables. Skipping the update of impedances overestimates losses (5.5%) because additional parallel lines reduce the total impedance. The lossy transport model underestimates losses (2.5%) since it neglects the quadratic relationship between power and losses. Table 2 further shows low curtailment at around 2% across all flow models due to generous line expansion allowances.

At first sight, the optimised technology mix appears relatively similar across all flow models, both in terms of cost composition in Figure 3 and the map of investments in Figure 6. This

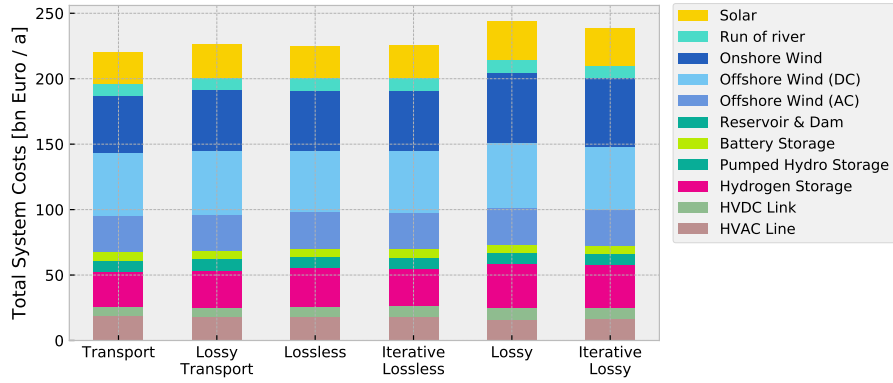


Figure 3: Comparison of total annual system costs split by system component for the covered flow models.

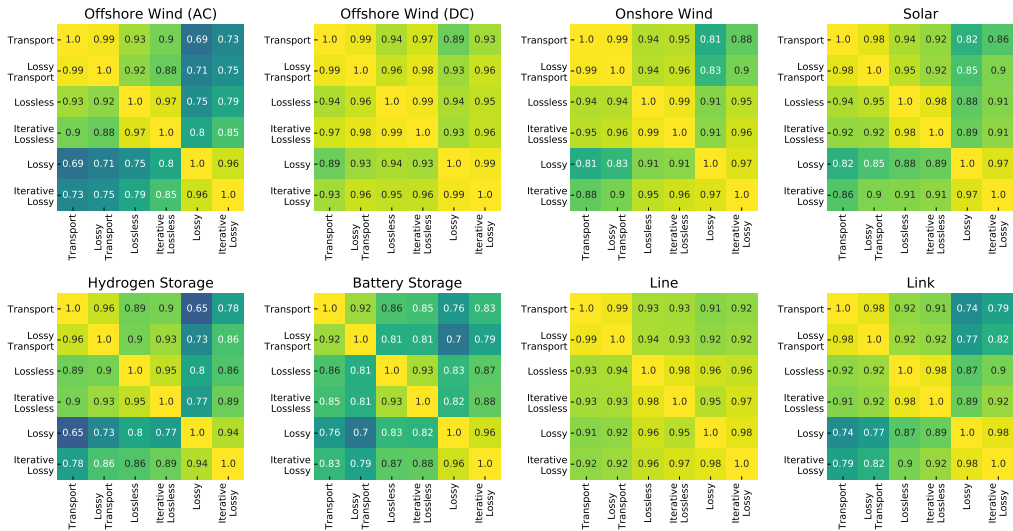


Figure 4: Capacity correlation of optimized nodal investments among covered flow models distinguished by technology.

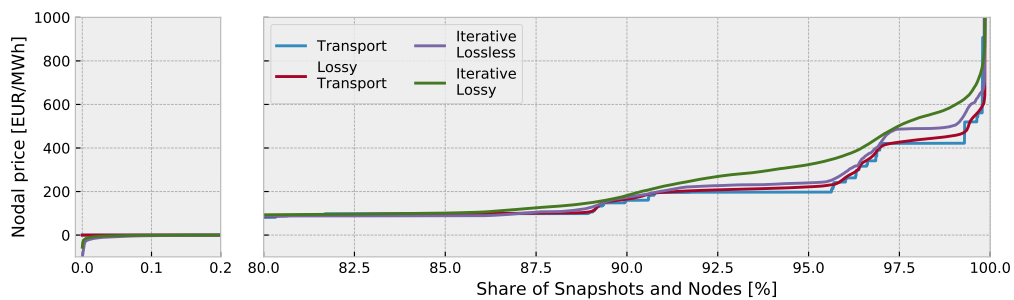


Figure 5: Nodal price duration curves (snapshots and nodes) for selected flow models. In the omitted section, prices rise steadily and similarly for all models. Some models allow for negative nodal prices with occurrence below 0.2%.

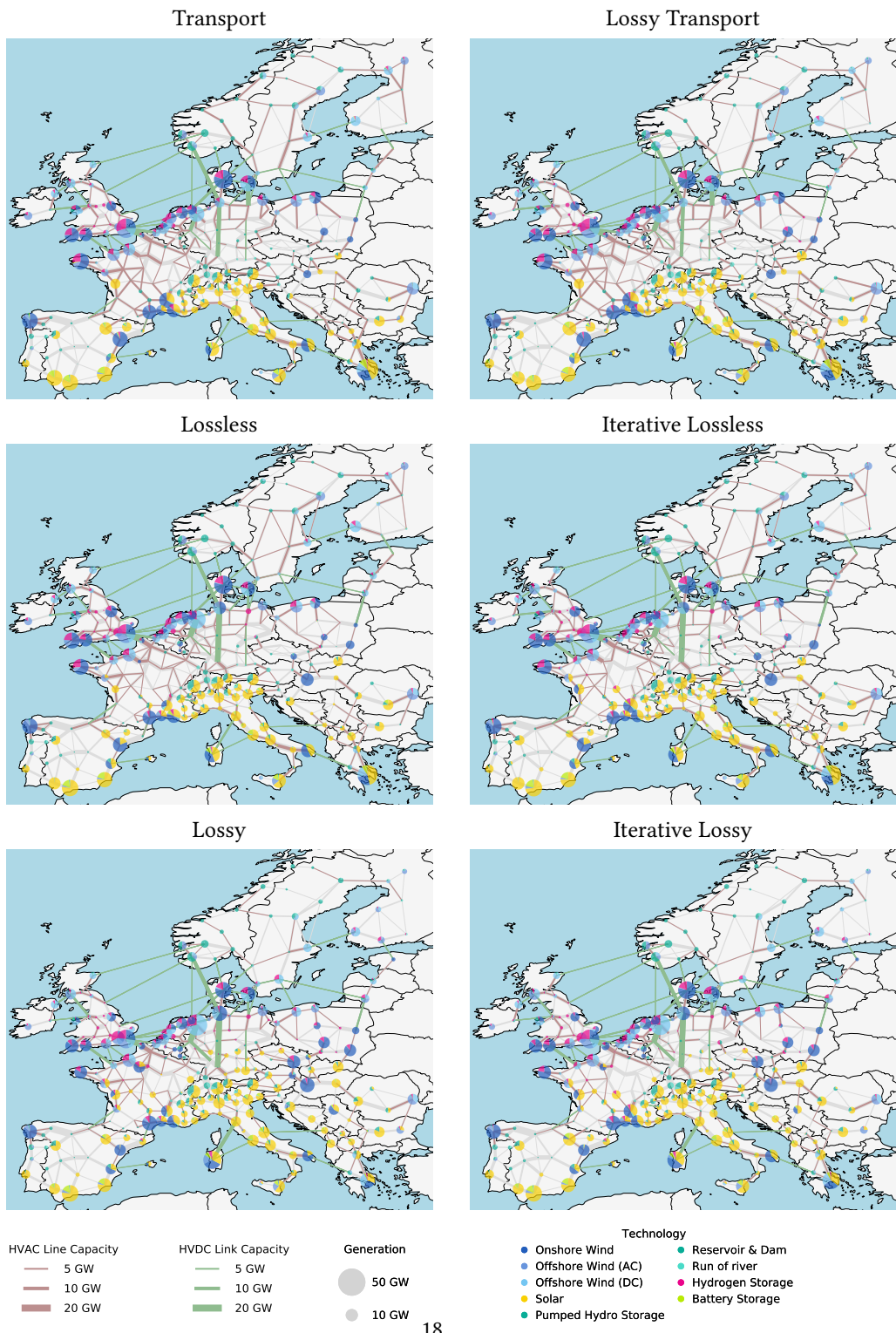


Figure 6: Maps of cost-optimal capacity expansion results for the covered lossless flow models.

is further underlined by the high correlations of optimised capacities shown in Figure 4. Potentially due to some placement degeneracies, lowest correlations are found for battery and hydrogen storage. Further notable differences concern grid reinforcement. The lossless and lossy transport models feature many new transmission lines in France and Scandinavia, which disappear as more accurate flow models are applied. The difference adds up to 20% less network reinforcement. Likewise, the energy transmitted decreases as more constraints are imposed on power transmission. In order to avoid grid losses, models that consider transmission losses and KVL transmitted up to 66% less energy than the transport model. The reduced spatial transport of power is then compensated by a shift towards hydrogen storage and controllable HVDC links (e.g. in the West of Germany). Despite the involved conversion losses, balancing renewables in time through storage becomes more attractive. Additionally, to offset the energy lost by transmission but also the reduced amount of power transmission, lossy models feature more wind and solar generation capacity. This includes both more localised generation (e.g. more solar panels in Southern Germany and more onshore wind turbines in Eastern Europe) where previously there were few production sites, and more concentrated generation in the North Sea region to pair with the appended storage units. The added capacities raise the system cost. In total, the annual system costs increase by approximately 5.7% compared to iterative linearised power flow, or 8% relative to the transport model.

Besides investments, we also compare electricity prices in an idealised nodal market by using the dual variables of the nodal balance constraints. The price duration curves depicted in Figure 5 show that nodal prices are more evenly distributed in the lossless linear power flow compared compared to the transport model. The even distribution of prices was also found in Gunkel et al. [17]. The transport model and lossy transport model do not have the properties that would allow negative prices. Negative nodal prices are a consequence of KVL and occur when increasing demand at a bus relieves a transmission line, allowing power to be exported from somewhere cheap to somewhere expensive. This lowers the system cost and consequently results in a negative price at that bus. Other constraints that can generally entail negative prices are unit commitment constraints, but these are not considered in this contribution. We find that even for models with KVL and loss approximations, negative prices are rare ($\leq 0.2\%$). The major differences regarding nodal prices can be observed in the 10% of highest prices. The transport model features step-like price profiles, whereas the profiles of the other models are smoother. The iterative lossy linearised power flow model possesses the highest yet smoothest price duration curve.

6.2. Validation of Loss Approximation

Figure 7 relates optimised line flows $p_{\ell,t}$ to optimised losses $\psi_{\ell,t}$ for the lossy transport model and the iterative lossy linearised power flow model. The lossy transport model underestimates losses under high loading conditions depending on the assumed constant loss factor and fails to reflect the quadratic relationship between losses and flow. On the contrary, the results also confirm that approximating losses in linearised optimal power flow with a convex envelope does not degrade the obtained solutions. Although the envelope around the loss parabola (38) (cf. Section 4.4, approximates cosine in (35)) allows for losses to take values above the parabola, the cost associated with losses tends to push losses downwards. Substantial deviations from the parabola to above only occur when there is no cost (or even a benefit in the case of negative nodal prices) associated with higher losses; e.g. when energy is being curtailed, or when there is some extra consumption of interest to control power flows or some other problem degeneracy. As previously shown in Figure 5, negative nodal prices and consequently incentives for loss

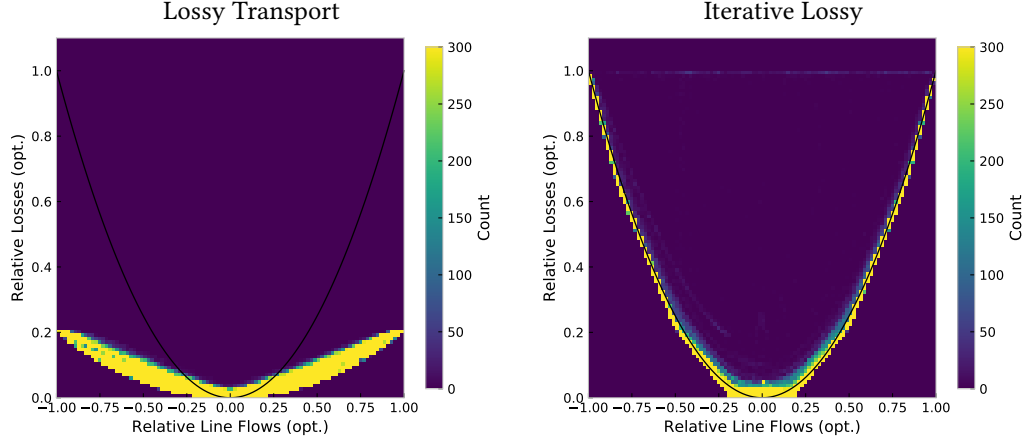


Figure 7: Examination of convex envelope relaxation around loss formula $\psi = rp^2$ given in equation (38) for lossy transport model and the iterative lossy linearised power flow model in a two-dimensional histogram. The line flows are normalised by their nominal capacity including the $N - 1$ security margin $(p_{\ell}, \bar{p}_{\ell}, P_{\ell})$ and maximum losses according to security-constrained line capacity respectively, such that lines with different electrical parameters can be mapped onto the same chart. The count refers to a tuple (ℓ, t) of line and snapshot. The black line depicts the normalised quadratic loss formula (38).

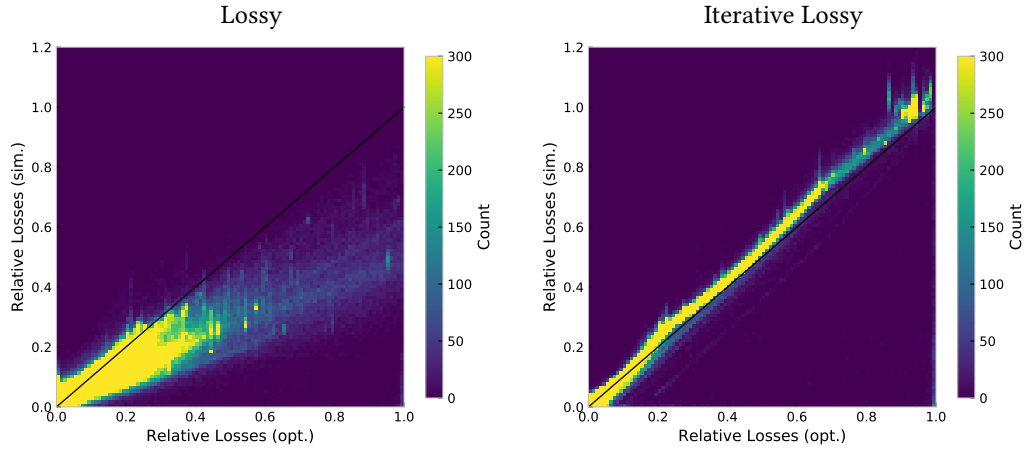


Figure 8: Comparison of simulated losses from AC power flow equations and optimised losses for iterative and non-iterative lossy linearised power flow in a two-dimensional histogram. Relative losses are shown as $\psi_{\ell, t} / \psi_{\ell, t}^{\max}$ according to security-constrained line capacity $\bar{p}_{\ell} P_{\ell}$. The count refers to a tuple (ℓ, t) of line and snapshot. The black line indicates perfect alignment of simulated and optimised losses.

Indicator	Unit	Lossy		Iterative		Iterative	
		Transport	Transport	Lossless	Lossless	Lossy	Lossy
Root Mean Squared (RMSE)	MW	1468	1059	790	679	298	60
Mean Absolute (MAE)	MW	775	707	269	207	194	35
Pearson Correlation (R)	-	0.91	0.94	0.97	0.98	0.99	0.998
Coef. of Determination (R^2)	-	0.83	0.89	0.94	0.95	0.98	0.996

Table 3: Flow errors compared across covered flow models.

overestimation are rare ($\leq 0.2\%$). These circumstances cause the generous convex relaxation to function well. Underestimating losses is also possible, albeit to a much smaller extent, as a small fraction of the feasible space lies between the loss parabola and the tangents that form the convex envelope. Recall that the loss parabola (38) is already an approximation of the cosine terms in equation (35).

Figure 8 compares transmission losses retrieved from the optimisation problem to the simulated losses from AC power flow for the iterating and non-iterating loss approximation. Like in Figure 7, we note that the iterative lossy formulation manages to sufficiently represent losses observed in the respective AC power flow simulation. However, when the iteration is skipped and hence line impedances are not updated according to their optimised capacities, losses are overestimated.

6.3. Validation of Optimised Line Flows

Figure 9 compares line flows from optimisation to simulated line flows from AC power flow for each of the flow models in a two-dimensional histogram. Figure 10 displays the same information from a different perspective as duration curves of relative line loading for both simulated and optimised flows (figure inspired by Brown et al. [19]). Table 3 quantifies the alignment of optimised and simulated flows with some standard absolute and relative measures of error that are frequently encountered in the literature (cf. [29]): root mean squared error (RMSE), mean average error (MAE), Pearson correlation coefficient (R), coefficient of determination (R^2).

First and foremost, the results reveal that the iterative lossy model matches simulated flows almost perfectly. Other formulations show deficiencies particularly under high loading conditions, but generally get the direction of flow right. The errors become significantly less pronounced and produce less undesired line overloading, the more physical characteristics of power flow are considered during optimisation. Limiting the utilisation of line capacities to 70% prevents abundant overloading. Remarkably, a high Pearson correlation coefficient of 0.91 is already achieved with the transport model, indicating that despite its simplicity the model can capture the dominant flow patterns we observe in the ex-post AC power flow simulation.

Lines with zero flow occur strikingly frequently in the lossy transport model, causing high deviations from the simulated flows. This can be explained with the aid of Figure 11. There are many cases where prices are (almost) the same at two neighbouring buses. In such cases, there is no strict economic need to move power between them. With a lossless transport model there is no penalty for moving power between the two nodes, such that the optimisation yields a random value. However, for the lossy transport there is an incentive to set the flow to zero to avoid the losses, which is why exactly this phenomenon frequently occurs when there is no price difference. The physical flow constraints enforced by KVL make it complicated to realise zero flow on a line. This is the reason why we do not observe many lines with zero flow for

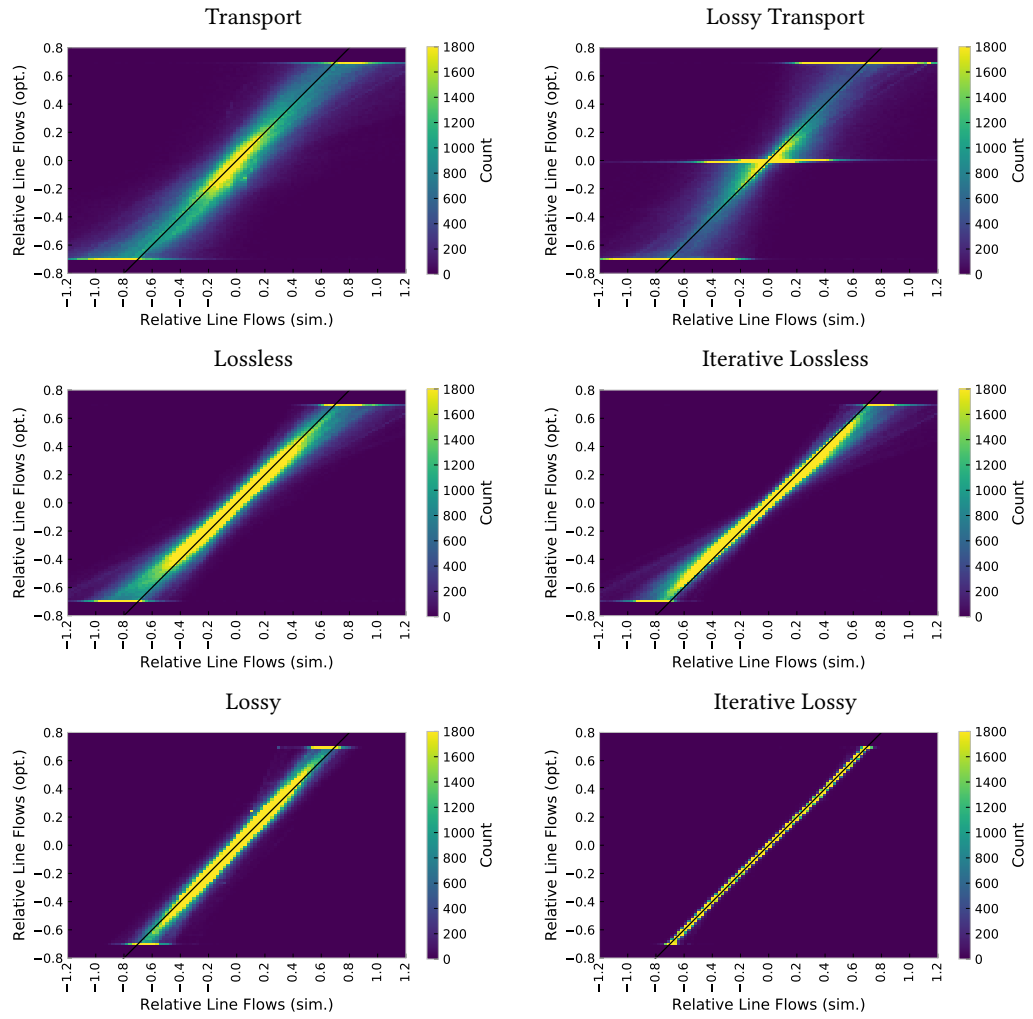


Figure 9: Two-dimensional histograms comparing simulated flows (AC power flow) and optimised flows of the indicated flow models. Relative line flows are shown as $p_{\ell,t}/P_{\ell}$. The count refers to a tuple (ℓ, t) of line and snapshot. The black line indicates perfect alignment of simulated and optimised flows.

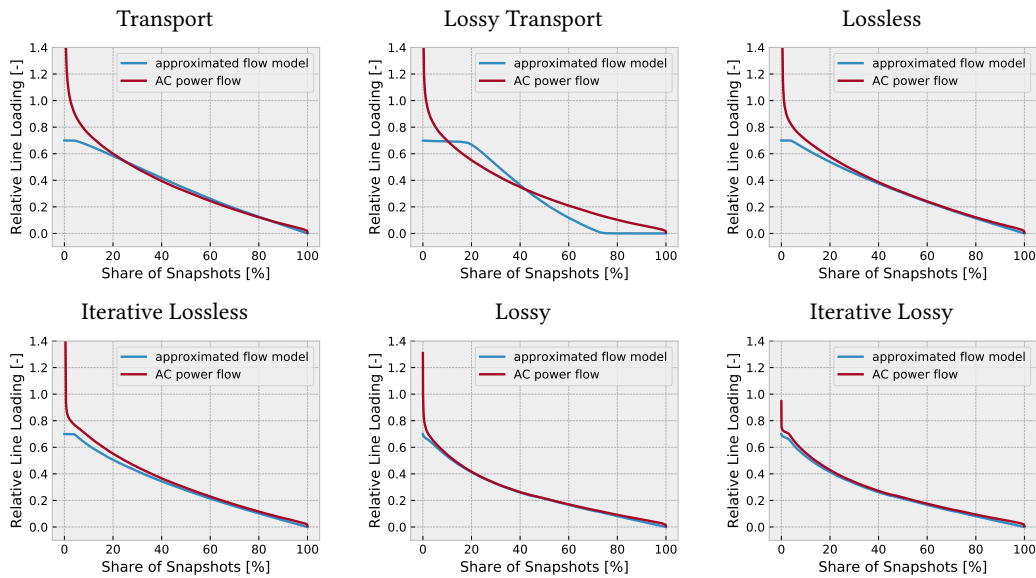


Figure 10: Flow duration curves of simulated flows (AC power flow) and optimised flows for the indicated flow models. Relative line loading is shown as $p_{\ell,t}/P_{\ell}$. The count refers to a tuple (ℓ, t) of line and snapshot.

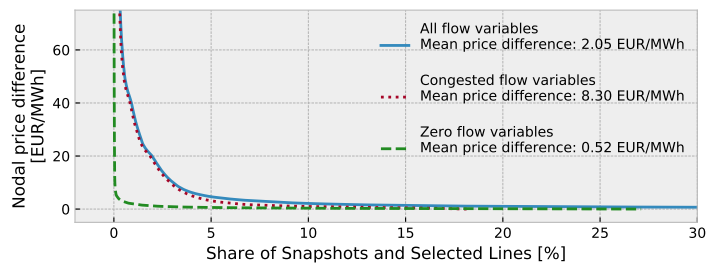


Figure 11: Duration curves (lines and snapshots) of nodal price differences for lines experiencing no flow, congested lines, and all lines.

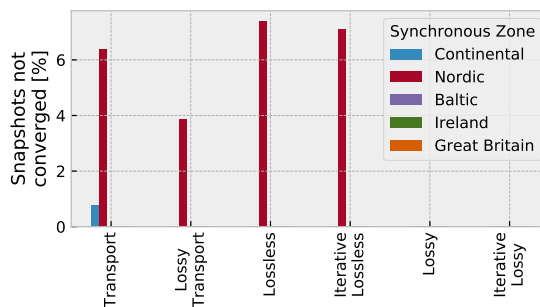


Figure 12: Share of snapshots where the Newton-Raphson algorithm for solving the AC power flow equations did not converge distinguished by colour-coded synchronous zone.

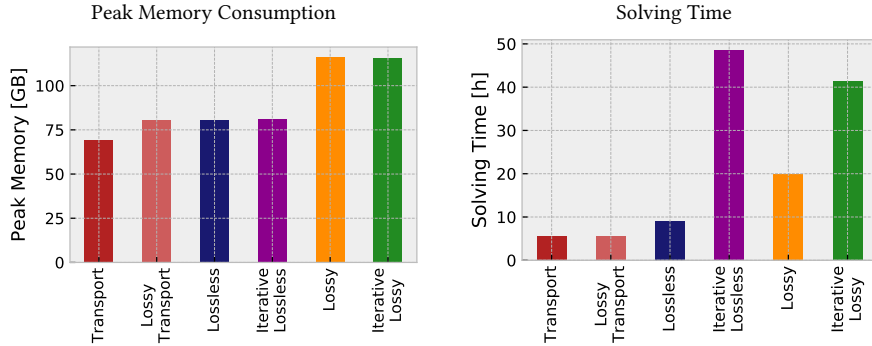


Figure 13: Comparison of computational performance in terms of peak memory consumption and solving time.

models that enforce KVL. Conversely, Figure 11 also shows that congested lines cause high nodal price differences.

In some cases the Newton-Raphson algorithm does not converge. Typical causes can be high voltage angle differences, voltage drops, and reactive power flows. The power flow simulation is run separately for each snapshot and each synchronous zone, so we can check individually what prevalent network characteristics, in combination with the underlying flow models, cause the failure to converge. The resulting share of snapshots not converged for each synchronous zone is presented in Figure 12. Almost exclusively, difficulties are observed in the Nordic synchronous zone which possesses many long (aggregated) lines, which lead to high voltage angle differences. With regard to the whole European system, the number of snapshots where no convergence is reached is low. We observe better convergence rates for more detailed flow models and the issue is found to become less problematic as the spatial resolution of the transmission network is increased.

Given that high voltage angle differences diminish the accuracy of the linear power flow approximation, a maximum of up to $\pm 30^\circ$ is commonly tolerated in the literature [28, 56, 57]. This domain links to the range beyond which the relative error of the small-angle approximation of the sine exceeds 5%. Since the cosine approximation is a second order Taylor series expansion, unlike the first order sine approximation, it does not reduce the acceptable range of angle differences further (cf. Table C.6). We observe that across all flow models a majority of voltage angle differences lies within an uncritically low range where the sine approximation is quite precise (cf. Figure C.14). The share of voltage angle differences outside $\pm 30^\circ$ reduces considerably with more physically accurate grid modelling (5% for transport model versus 1.5% for lossy model, cf. Table 2).

6.4. Computational Performance

The computational performance of the different flow models, both in terms of memory and computation time, is shown in Figure 13. More variables and constraints leads to higher peak memory consumption. The spectrum ranges from 70 GB to 130 GB (around factor 2). Particularly the loss approximation raises memory requirements significantly in relation to added KVL constraints or constant efficiencies, also depending on the number of tangents used for the convex envelope. Solving times range between 5 hours and 50 hours (factor 10). Lossy and lossless transport model are solved the fastest by far. The lossless linearised power flow model

requires almost twice the time. Iteration has the biggest impact on solving times, multiplying with the number of iterations. Finally, we notice that the lossy formulations are more prone to numerical issues, which could be circumvented by increasing the numeric accuracy parameter of the solver at the cost of computational speed.

6.5. Critical Appraisal

The disregard of voltages and reactive power flows during optimisation ranks among the severest shortcomings of the presented flow models. The cost and required capacities for reactive power control are not assessed. The confinement to linear formulations may also be considered as a weakness in view of recent developments in convex second-order cone solvers.

Additionally, we consider the high-voltage transmission network only and do not assess the performance of flow models in low-voltage distribution grids. This is especially relevant in view of further closing the granularity gap. Furthermore, losses on the distribution level are not directly modelled but taken into account only through the electricity demand. Typically, the scale of losses is higher than at the transmission level, as for instance the German Federal Network Agency reports [55]. In 2019, losses at the transmission level amounted to 1.2%, whereas losses at the distribution level were as high as 3%. Moreover, the relations between ambient temperature, dynamic line rating and losses are not addressed. Higher ambient temperatures reduce the amount of power a transmission line can transmit safely but simultaneously increase the resistance, affecting the losses.

Although the clustered transmission system is of course also simplified due to computational constraints, we could observe consistent results for spatial aggregation to 100, 200 and 250 nodes. However, the extent of network clustering also affects the length of modelled lines and we note that for very long lines with voltage angle differences beyond $\pm 30^\circ$ in highly aggregated grid models the standard equivalent Π model may not be suitable [53].

7. Conclusion

In the present contribution we discuss best practices for incorporating two inherently non-linear phenomena, power flow and transmission losses, into linear capacity expansion problems that co-optimize investments in generation, storage and transmission infrastructure.

High model fidelity comes at the cost of high computational burden. Given the cross-disciplinary nature of energy system modelling and differences in complexity, the selection of a suitable representation of power flows depends on the application, the user's availability of computational resources, and the level of spatial detail considered. A highly aggregated network will not benefit from detailed power flow modelling, whereas modelling losses is critical in the presence of continent-spanning power transmission at sub-national detail. The present paper provides a detailed comparison to facilitate this choice.

We find that already as little as three tangents are sufficient to accurately approximate the quadratic losses, which in turn are an approximation of the trigonometric losses. We do not observe excessive fictitious losses despite the broad convex relaxation. However, we conclude that accounting for changing impedances as lines are expanded is essential. Otherwise, losses will be overestimated.

The literature predominantly employs the lossless transport model in design studies, which can already capture the main features of a cost-efficient system, but is too inexact for subsequent nonlinear power flow calculations. However, a representation of power flows that considers

transmission losses as well as both Kirchhoff laws allows us to bridge between techno-economic models and more detailed electrotechnical models.

Acknowledgement

F.N. and T.B. gratefully acknowledge funding from the Helmholtz Association under grant no. VH-NG-1352. The responsibility for the contents lies with the authors. This work is licensed under a [Creative Commons “Attribution 4.0 International”](#) license. 

CRedit Author Statement

Fabian Neumann: Conceptualization, Methodology, Investigation, Software, Validation, Formal analysis, Visualization, Writing – Original Draft, Writing – Review & Editing **Veit Hagenmeyer:** Writing – Review & Editing, Project administration, Funding acquisition **Tom Brown:** Conceptualization, Writing – Review & Editing, Supervision, Project administration, Funding acquisition

Data Availability

A dataset of the results including networks and graphics is available abstract doi.org/10.5281/zenodo.3968297. We also refer to the documentation of PyPSA (pypsa.readthedocs.io), PyPSA-Eur (pypsa-eur.readthedocs.io) and the source code repository (github.com/fneum/power-flow-models).

References

- [1] T. Brown, D. Schlachtberger, A. Kies, S. Schramm, M. Greiner, Synergies of sector coupling and transmission reinforcement in a cost-optimised, highly renewable european energy system, *Energy* 160 (2018) 720 – 739, arXiv:1801.05290. [doi: 10/gfdstr](https://doi.org/10.1016/j.energy.2018.05.032).
- [2] V. Krishnan, J. Ho, B. F. Hobbs, A. L. Liu, J. D. McCalley, M. Shahidehpour, Q. Zheng, Co-optimization of electricity transmission and generation resources for planning and policy analysis: review of concepts and modeling approaches, *Energy Systems* 7 (2016) 297–332. [doi: 10/d3bd](https://doi.org/10.1016/j.iesys.2016.05.001).
- [3] L. Kotzur, P. Markewitz, M. Robinius, D. Stolten, Impact of different time series aggregation methods on optimal energy system design, *Renewable Energy* 117 (2018) 474 – 487, arXiv:1708.00420. [doi: 10/d3bc](https://doi.org/10.1016/j.renene.2018.03.032).
- [4] L. Kotzur, P. Markewitz, M. Robinius, D. Stolten, Time series aggregation for energy system design: Modeling seasonal storage, *Applied Energy* 213 (2018) 123 – 135, arXiv:1710.07593. [doi: 10/gc5jn8](https://doi.org/10.1016/j.apenergy.2018.03.032).
- [5] J. Hrsch, T. Brown, [The role of spatial scale in joint optimisations of generation and transmission for European highly renewable scenarios](#), 14th International Conference on the European Energy Market ArXiv:1705.07617 (2017). URL <https://arxiv.org/abs/1705.07617>
- [6] D. P. Schlachtberger, T. Brown, S. Schramm, M. Greiner, The Benefits of Cooperation in a Highly Renewable European Electricity Network, *Energy* 134 (2017) 469–481, arXiv:1704.05492. [doi: 10/gbvpcf](https://doi.org/10.1016/j.energy.2017.04.032).
- [7] C. Nolden, M. Schonfelder, A. Esser-Frey, V. Bertsch, W. Fichtner, Network constraints in techno-economic energy system models: towards more accurate modeling of power flows in long-term energy system models, *Energy Systems* 4 (3) (2013) 267–287. [doi: 10/ggtk2h](https://doi.org/10.1016/j.iesys.2013.05.001).
- [8] S. Lumberras, A. Ramos, F. Banez Chicharro, Optimal transmission network expansion planning in real-sized power systems with high renewable penetration, *Electric Power Systems Research* 149 (2017) 76–88. [doi: 10/gbqp9m](https://doi.org/10.1016/j.epsr.2017.05.001).
- [9] D. Bienstock, A. Verma, Strong NP-hardness of AC power flows feasibility, *Operations Research Letters* 47 (6) (2019) 494 – 501, arXiv:1512.07315v1. [doi: 10/d299](https://doi.org/10.1016/j.orl.2019.05.001).
- [10] K. Lehmann, A. Grastien, P. V. Hentenryck, AC-feasibility on tree networks is NP-hard, *IEEE Transactions on Power Systems* 31 (1) (2016) 798–801. [doi: 10/d3bb](https://doi.org/10.1109/TPWRS.2015.2444444).

- [11] S. Sojoudi, J. Lavaei, Physics of power networks makes hard optimization problems easy to solve, in: IEEE Power and Energy Society General Meeting, 2012, pp. 1–8. [doi:10/ggbgnc](https://doi.org/10/ggbgnc).
- [12] F. Neumann, T. Brown, Heuristics for transmission expansion planning in low-carbon energy system models, in: 16th International Conference on the European Energy Market, 2019, pp. 1–8, arXiv:1907.10548. [doi:10/d295](https://doi.org/10/d295).
- [13] K.-K. Cao, K. von Krbeke, M. Wetzel, F. Cebulla, S. Schreck, Classification and evaluation of concepts for improving the performance of applied energy system optimization models, *Energies* 12 (24) (2019) 4656. [doi:10/ggd8rf](https://doi.org/10/ggd8rf).
- [14] H.-K. Ringkjøb, P. M. Haugan, I. M. Solbrekke, A review of modelling tools for energy and electricity systems with large shares of variable renewables, *Renewable and Sustainable Energy Reviews* 96 (2018) 440–459. [doi:10/gfgb5g](https://doi.org/10/gfgb5g).
- [15] W. Nijs, S. Simoes, A. Sgobbi, P. Ruiz-Castello, C. Thiel, G. Giannakidis, J. Mantzaris, K. Tigas, D. Dimitroulas, P. Georgilakis, C. Vournas, Improved representation of the European power grid in long term energy system models: Case study of JRC-EU-TIMES, in: G. Giannakidis, M. Labriet, B. O Gallachoir, G. Tosato (Eds.), *Informing Energy and Climate Policies Using Energy Systems Models*, Vol. 30, Springer International Publishing, 2015, pp. 201–222. [doi:10/d297](https://doi.org/10/d297).
- [16] M. Haller, S. Ludig, N. Bauer, Bridging the scales: A conceptual model for coordinated expansion of renewable power generation, transmission and storage, *Renewable and Sustainable Energy Reviews* 16 (5) (2012) 2687–2695. [doi:10/f335pp](https://doi.org/10/f335pp).
- [17] P. A. Gunkel, H. Koduvere, J. G. Kirkerud, F. J. Fausto, H. Ravn, Modelling transmission systems in energy system analysis: A comparative study, *Journal of Environmental Management* 262 (2020) 110289. [doi:10/ggq4mb](https://doi.org/10/ggq4mb).
- [18] K. Schaber, *Integration of variable renewable energies in the European power system: a model-based analysis of transmission grid extensions and energy sector coupling*, PhD thesis, Technical University Munich, Munich, Germany (Dec. 2013).
URL <https://mediatum.ub.tum.de/doc/1163646/document.pdf>
- [19] T. Brown, E. Trster, P.-P. Schierhorn, T. Ackermann, Optimising the European transmission system for 77% renewable electricity by 2030, *IET Renewable Power Generation* 10 (1) (2016) 3–9. [doi:10/f75tr3](https://doi.org/10/f75tr3).
- [20] D. Z. Fitiwi, L. Olmos, M. Rivier, F. de Cuadra, I. J. Prez-Arriaga, Finding a representative network losses model for large-scale transmission expansion planning with renewable energy sources, *Energy* 101 (2016) 343–358. [doi:10/f8k3ww](https://doi.org/10/f8k3ww).
- [21] B. Stott, J. Jardim, O. Alsa, DC power flow revisited, *IEEE Transactions on Power Systems* 24 (3) (2009) 1290–1300. [doi:10/c8sx2b](https://doi.org/10/c8sx2b).
- [22] J. Hörsch, F. Hofmann, D. Schlachtberger, T. Brown, PyPSA-Eur: An open optimisation model of the European transmission system, *Energy Strategy Reviews* 22 (2018) 207–215, arXiv:1806.01613. [doi:10/d294](https://doi.org/10/d294).
- [23] S. Pfenninger, A. Hawkes, J. Keirstead, Energy systems modeling for twenty-first century energy challenges, *Renewable and Sustainable Energy Reviews* 33 (2014) 74–86. [doi:10/f526xf](https://doi.org/10/f526xf).
- [24] J. DeCarolis, H. Daly, P. Dodds, I. Keppo, F. Li, W. McDowall, S. Pye, N. Strachan, E. Trutnevte, W. Usher, M. Winning, S. Yeh, M. Zeyringer, Formalizing best practice for energy system optimization modelling, *Applied Energy* 194 (2017) 184–198. [doi:10/f96rdx](https://doi.org/10/f96rdx).
- [25] B. Hobbs, G. Drayton, E. Bartholomew Fisher, W. Lise, Improved transmission representations in oligopolistic market models: quadratic losses, phase shifters, and DC lines, *IEEE Transactions on Power Systems* 23 (3) (2008) 1018–1029. [doi:10/b4df8d](https://doi.org/10/b4df8d).
- [26] S. Hagspiel, C. Jagemann, D. Lindenberger, T. Brown, S. Cherevatskiy, E. Tröster, Cost-optimal power system extension under flow-based market coupling, *Energy* 66 (2014) 654–666. [doi:10/f5zsq4](https://doi.org/10/f5zsq4).
- [27] J. A. Taylor, *Convex Optimization of Power Systems*, Cambridge University Press, 2015.
- [28] F. Dörfler, F. Bullo, Novel insights into lossless ac and dc power flow, in: 2013 IEEE Power Energy Society General Meeting, IEEE, 2013. [doi:10/d6z4](https://doi.org/10/d6z4).
- [29] C. Coffrin, P. V. Hentenryck, R. Bent, Approximating line losses and apparent power in AC power flow linearizations, in: 2012 IEEE Power and Energy Society General Meeting, IEEE, 2012. [doi:10/ggfzwr](https://doi.org/10/ggfzwr).
- [30] D. K. Molzahn, I. A. Hiskens, A survey of relaxations and approximations of the power flow equations, *Foundations and Trends in Electric Energy Systems* 4 (1-2) (2019) 1–221. [doi:10/d298](https://doi.org/10/d298).
- [31] C. Coffrin, L. Roald, *Convex Relaxations in Power System Optimization: A Brief Introduction* ArXiv:1807.07227 (Jul. 2018).
URL <http://arxiv.org/abs/1807.07227>
- [32] C. Coffrin, P. Van Hentenryck, A linear-programming approximation of AC power flows, *INFORMS Journal on Computing* 26 (4) (2014) 718–734. [doi:10/f6km6h](https://doi.org/10/f6km6h).
- [33] J. Hörsch, H. Ronellenfitch, D. Witthaut, T. Brown, Linear optimal power flow using cycle flows, *Electric Power Systems Research* 158 (2018) 126–135, arXiv:1704.01881. [doi:10/gdb8kx](https://doi.org/10/gdb8kx).
- [34] R. K. Ahuja, T. L. Magnanti, J. B. Orlin, *Network Flows: Theory, Algorithms, and Applications*, Prentice Hall, New Jersey, 1993.
- [35] F. Neumann, T. Brown, Transmission expansion planning using cycle flows, in: *Proceedings of the Eleventh ACM*

- International Conference on Future Energy Systems, e-Energy fi20, Association for Computing Machinery, New York, NY, USA, 2020, p. 253fi?!263, arXiv:2004.08702. doi: 10/d3qk.
- [36] J. W. Simpson-Porco, Lossy DC power flow, IEEE Transactions on Power Systems 33 (3) (2018) 2477–2485, arXiv:1611.05953. doi: 10/gdgqrr.
- [37] H. Zhang, V. Vittal, G. T. Heydt, J. Quintero, A relaxed AC optimal power flow model based on a Taylor series, IEEE Innovative Smart Grid Technologies Asia (2013) 5–9doi: 10/d296.
- [38] H. Zhang, G. T. Heydt, V. Vittal, J. Quintero, An improved network model for transmission expansion planning considering reactive power and network losses, IEEE Transactions on Power Systems 28 (3) (2013) 3471–3479. doi: 10/f472bm.
- [39] P. Sanchez-Martin, A. Ramos, Modeling transmission ohmic losses in a stochastic bulk production cost model (2006). URL <https://tinyurl.com/y67t9dvh>
- [40] H. Farahmand, D. Huertas-Hernando, L. Warland, M. Korpas, H. G. Svendsen, Impact of system power losses on the value of an offshore grid for North Sea offshore wind, in: 2011 IEEE Trondheim PowerTech, IEEE, 2011, pp. 1–7. doi: 10/cnmx9d.
- [41] Electric Power Research Institute, Program on Technology Innovation: Coordinated Expansion Planning: Status and Research Challenges, Tech. Rep. 3012016661, Palo Alto, CA (Dec. 2019). URL https://www.vibrantcleanenergy.com/wp-content/uploads/2019/12/EPRI_Report_Dec2019.pdf
- [42] T. N. dos Santos, A. L. Diniz, A dynamic piecewise linear model for DC transmission losses in optimal scheduling problems, IEEE Transactions on Power Systems 26 (2) (2011) 508–519. doi: 10/b5rk9g.
- [43] P. Fortenbacher, T. Demiray, Linear/quadratic programming-based optimal power flow using linear power flow and absolute loss approximationsArxiv:1711.00317 (2017). doi: 10/gd6svt.
- [44] R. Palma-Benhke, A. Philpott, A. Jofr, M. Corts-Carmona, Modelling network constrained economic dispatch problems, Optimization and Engineering 14 (3) (2013) 417–430. doi: 10/ggq5gt.
- [45] Z. Yang, H. Zhong, A. Bose, T. Zheng, Q. Xia, C. Kang, A linearized OPF model with reactive power and voltage magnitude: a pathway to improve the MW-Only DC OPF, IEEE Transactions on Power Systems 33 (2) (2018) 1734–1745. doi: 10/gc5jrd.
- [46] H. Zhong, Q. Xia, Y. Wang, C. Kang, Dynamic economic dispatch considering transmission losses using quadratically constrained quadratic program method, IEEE Transactions on Power Systems 28 (3) (2013) 2232–2241. doi: 10/gfzp35.
- [47] T. Brown, T. Bischof-Niemz, K. Blok, C. Breyer, H. Lund, B. Mathiesen, Response to fiBurden of proof: A comprehensive review of the feasibility of 100% renewable-electricity systemsfi, Renewable and Sustainable Energy Reviews 92 (2018) 834 – 847. doi: 10/gdwmvw.
- [48] Siemens, HVDC Classic – powerful and economical: High-performance power transmission, Tech. rep. (2017). URL <https://tinyurl.com/yy3ouxwm>
- [49] ENTSO-E, Ten year network development plan (TYNDP), Tech. rep. (2018). URL <https://tyndp.entsoe.eu/tyndp2018/tyndp2018>
- [50] T. Brown, J. Hörsch, D. Schlachtberger, PyPSA: Python for Power System Analysis, Journal of Open Research Software 6 (2018) 4, arXiv:1707.09913. doi: 10/gfb7m9.
- [51] J. J. Grainer, W. Stevenson, Power System Analysis, McGraw-Hill, 1994.
- [52] F. Milano, PSAT documentation: version 2.0.0, Tech. rep. (feb 2008). URL <https://www.eecs.wsu.edu/~ee521/Material/20120927/psat-20080214.pdf>
- [53] P. Kundur, Power System Stability and Control, McGraw-Hill, 1994.
- [54] J. Machowski, J. Bialek, J. Bumby, Power System Dynamics: Stability and Control, 2nd Edition, Wiley-Blackwell, 2008.
- [55] German Federal Network Agency (Bundesnetzagentur), Monitoring report 2019, Tech. rep. (nov 2019). URL <https://www.bundesnetzagentur.de/SharedDocs/Downloads/EN/Areas/ElectricityGas/CollectionCompanySpecificData/Monitoring/MonitoringReport2019.pdf>
- [56] K. Dvijotham, D. K. Molzahn, Error bounds on the DC power flow approximation: A convex relaxation approach, in: 2016 IEEE 55th Conference on Decision and Control (CDC), 2016, pp. 2411–2418. doi: 10/d64w.
- [57] K. Purchala, L. Meeus, D. Van Dommelen, R. Belmans, Usefulness of DC power flow for active power flow analysis, in: IEEE Power Engineering Society General Meeting, 2005, 2005, pp. 454–459. doi: 10/d4ww62.

Appendix A. AC Power Flow Problem Solved with Newton-Raphson

Appendix A.1. Without Distributed Slack

Given nodal power imbalances S_n at any given snapshot for each bus n the AC power flow equations are given by

$$S_n = P_n + iQ_n = V_n I_n^* = V_n \left(\sum_m Y_{nm} V_m \right)^*, \quad (\text{A.1})$$

where $V_n = |V_n| e^{i\theta_n}$ is the complex voltage, whose rotating angle is taken relative to the slack bus and Y_{nm} is the bus admittance matrix, based on the branch impedances and shunt admittances (including those attached to buses).

For the slack bus $n = 0$ it is assumed $|V_0|$ is given and that $\theta_0 = 0$; P and Q are to be found. For the PV buses, P and $|V|$ are given; Q and θ are to be found. For the PQ buses, P and Q are given; $|V|$ and θ are to be found.

Considering PV and PQ as sets of buses, then there are $|\text{PV}| + 2|\text{PQ}|$ real-valued equations to solve:

$$\text{Re} \left[V_n \left(\sum_m Y_{nm} V_m \right)^* \right] - P_n = 0 \quad \forall \text{PV} \cup \text{PQ} \quad (\text{A.2})$$

$$\text{Im} \left[V_n \left(\sum_m Y_{nm} V_m \right)^* \right] - Q_n = 0 \quad \forall \text{PQ} \quad (\text{A.3})$$

We need to find θ_n for all PV and PQ buses and $|V_n|$ for all PQ buses.

These equations $f(x) = 0$ are solved using the Newton-Raphson method, with the Jacobian

$$\frac{\partial f}{\partial x} = \begin{pmatrix} \frac{\partial P}{\partial \theta} & \frac{\partial P}{\partial |V|} \\ \frac{\partial Q}{\partial \theta} & \frac{\partial Q}{\partial |V|} \end{pmatrix} \quad (\text{A.4})$$

and the initial guesses $\theta_n = 0$ and $|V_n| = 1$ for unknown quantities. For more details see for example Grainger and Stevenson [51]. The total active slack power, which balances remaining mismatches of power generation and demand resulting from the AC power flow equations, is fully allocated to the slack bus. This can be a crude assumption, particularly for large networks with a high penetration of renewables.

Appendix A.2. With Distributed Slack

A better alternative is to distribute the total active slack power across all generators in proportion to their capacities (or another distribution scheme) [52]. The active power flow equations are altered to

$$\text{Re} \left[V_n \left(\sum_m Y_{nm} V_m \right)^* \right] - P_n - P_{\text{slack}} \gamma_n = 0 \quad \forall \text{PV} \cup \text{PQ} \cup \text{slack} \quad (\text{A.5})$$

where P_{slack} is the total slack power and γ_n is the share of bus n of the total generation capacity, which is used as distribution key. We add an additional active power balance equation for the slack bus since it is now part of the distribution scheme.

The distributed slack approach extends the Jacobian by an additional row for the derivatives of the slack bus active power balance and by an additional column for the partial derivatives with respect to γ

$$\frac{\partial f}{\partial x} = \begin{pmatrix} \frac{\partial P_0}{\partial \theta} & \frac{\partial P_0}{\partial |V|} & \frac{\partial P_0}{\partial \gamma} \\ \frac{\partial P}{\partial \theta} & \frac{\partial P}{\partial |V|} & \frac{\partial P}{\partial \gamma} \\ \frac{\partial Q}{\partial \theta} & \frac{\partial Q}{\partial |V|} & \frac{\partial Q}{\partial \gamma} \end{pmatrix}. \quad (\text{A.6})$$

If $\gamma_n = 0$ for all buses but the slack bus, this is equivalent to a single slack bus model.

Appendix B. Relations between Electrical Line Parameters

Following e.g. [51], the complex per-unit impedance $z_\ell = r_\ell + ix_\ell$ is composed of ohmic resistance r_ℓ and reactance x_ℓ . Likewise, the admittance $y_\ell = g_\ell + ib_\ell$ is composed of conductance g_ℓ and susceptance b_ℓ . Impedance and admittance are reciprocals ($y_\ell = z_\ell^{-1}$), hence we obtain the relations

$$g_\ell + ib_\ell = \frac{1}{r_\ell + ix_\ell}, \quad (\text{B.1})$$

$$g_\ell + ib_\ell = \frac{r_\ell - ix_\ell}{(r_\ell + ix_\ell)(r_\ell - ix_\ell)}, \quad (\text{B.2})$$

$$g_\ell + ib_\ell = \frac{r_\ell - ix_\ell}{r_\ell^2 + x_\ell^2}. \quad (\text{B.3})$$

By splitting real and imaginary parts we can express conductance and susceptance in terms of impedance and reactance:

$$g_\ell = \text{Re} \left[\frac{r_\ell - ix_\ell}{r_\ell^2 + x_\ell^2} \right] = \frac{r_\ell}{r_\ell^2 + x_\ell^2}, \quad (\text{B.4})$$

$$b_\ell = \text{Im} \left[\frac{r_\ell - ix_\ell}{r_\ell^2 + x_\ell^2} \right] = \frac{-x_\ell}{r_\ell^2 + x_\ell^2}. \quad (\text{B.5})$$

Appendix C. Additional Figures and Tables

Labels for used mathematical symbols are included in Table [Appendix C](#). An overview of applied assumptions in selected equations of the present paper is given in Table [C.5](#). Histograms of voltage angle differences for the evaluated flow models are plotted in Figure [C.14](#). Relative errors of first and second order small-angle approximations of trigonometric functions are listed in Table [C.6](#). Information on the distribution of line lengths in the considered network are displayed in Figure [C.15](#). Optimised capacities and energy generation by carrier are summarised in Table [C.7](#) and Table [C.8](#).

Symbol	Description
\mathcal{N}	set of buses
\mathcal{L}	set of lines
\mathcal{C}	set of cycles in cycle basis
g_ℓ	conductance
b_ℓ	susceptance
r_ℓ	resistance
x_ℓ	reactance
z_ℓ	impedance
y_ℓ	admittance
$ V_i $	voltage magnitude
θ_i	voltage angle
$p_{\ell(i,j)} = p_\ell$	active power flow
$q_{\ell(i,j)} = q_\ell$	reactive power flow
ψ_ℓ	power loss
$K_{i\ell}$	incidence matrix
$C_{\ell c}$	cycle incidence matrix
p_i	nodal power injection
P_ℓ	line capacity
\bar{P}_ℓ	maximum line capacity
\bar{p}_ℓ	maximum per-unit flow
m_k	slope of loss tangent for interval k
a_k	offset of loss tangent for interval k
n	number of intervals for loss tangents

Table C.4: Nomenclature

Formulas	Assumptions	$ V_i \approx 1$	$b_\ell \gg g_\ell$	$x_\ell \gg r_\ell$	$\sin(\theta_i - \theta_j) \approx \theta_i - \theta_j$	$\cos(\theta_i - \theta_j) \approx 1 - \frac{(\theta_i - \theta_j)^2}{2}$	$q_\ell = 0$
$g_\ell \approx r_\ell x_\ell^{-2}$	(21)			x			
$b_\ell \approx x_\ell^{-1}$	(22)			x			
$p_\ell = b_\ell(\theta_i - \theta_j)$	(27)	x	x		x		x
$\sum_\ell C_{\ell c} p_\ell b_\ell^{-1} = 0$		x	x		x		x
$p_\ell = x_\ell^{-1}(\theta_i - \theta_j)$	(28)	x	x	x	x		x
$\sum_\ell C_{\ell c} p_\ell x_\ell = 0$	(31)	x	x	x	x		x
$\psi_\ell = 2g_\ell[1 - \cos(\theta_i - \theta_j)]$	(34)	x					x
$\psi_\ell = 2g_\ell[1 - \cos(p_\ell b_\ell^{-1})]$		x	x		x		x
$\psi_\ell = 2r_\ell x_\ell^{-2}[1 - \cos(p_\ell x_\ell)]$	(35)	x	x	x	x		x
$\psi_\ell = r_\ell p_\ell^2$	(38)	x	x	x	x	x	x

Table C.5: Overview of applied assumptions in respective equations.

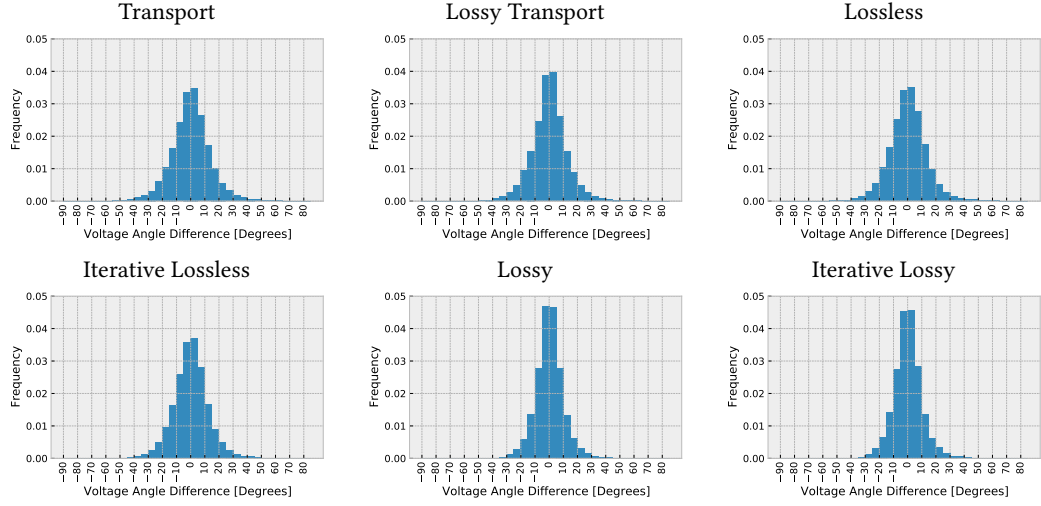


Figure C.14: Distribution of voltage angle differences for the indicated flow models.

$\theta_i - \theta_j$	$\sin(\theta_i - \theta_j) \approx \theta_i - \theta_j$	$\cos(\theta_i - \theta_j) \approx 1 - \frac{(\theta_i - \theta_j)^2}{2}$
$\pm 10^\circ$	0.5%	0.0%
$\pm 20^\circ$	2.1%	0.1%
$\pm 30^\circ$	4.7%	0.4%
$\pm 40^\circ$	8.6%	1.3%

Table C.6: Relative error of small-angle approximations by angle.

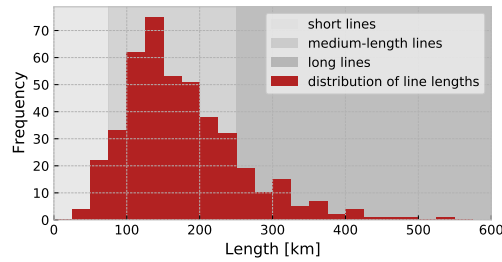


Figure C.15: Distribution of line lengths in 250 node networks by line classification according to Kundur [53]. Of all lines, 15% fall into the category of long lines, while 6% are classified as short lines.

Carrier	Unit	Transport	Lossy		Iterative		Iterative
			Transport	Lossless	Lossless	Lossy	
Offshore Wind (AC)	GW	139	137	139	137	141	135
Offshore Wind (DC)	GW	209	215	207	208	217	212
Onshore Wind	GW	328	346	343	347	401	393
Run of River	GW	34	34	34	34	34	34
Solar	GW	431	461	440	456	535	517
Pumped Hydro	GW	55	55	55	55	55	55
Hydro Dam	GW	100	100	100	100	100	100
Hydrogen Storage	GW	121	128	131	127	150	146
Battery Storage	GW	47	45	44	46	42	43
HVDC Links	TWkm	48	45	60	63	69	67
HVAC Lines	TWkm	167	160	146	143	91	103

Table C.7: Optimised capacities by technology for different flow models.

Carrier	Unit	Transport	Lossy		Iterative		Iterative
			Transport	Lossless	Lossless	Lossy	
Offshore Wind (AC)	TWh	525	515	526	515	509	504
Offshore Wind (DC)	TWh	935	967	922	927	983	953
Onshore Wind	TWh	875	908	907	901	988	980
Run of River	TWh	139	140	139	138	140	140
Solar	TWh	510	539	508	521	586	576
Hydro Inflow	TWh	387	387	387	387	387	387

Table C.8: Energy by carrier for different flow models.